Inorg. Chem. **2009**, *48*, 2277−2284

CeAsSe—Synthesis, Crystal Structure, and Physical Properties

A. Schlechte,[†] R. Niewa,*[,‡] Yu. Prots,[†] W. Schnelle,[†] M. Schmidt,[†] and R. Kniep[†]

Max-Planck-Institut für Chemische Physik fester Stoffe, 01187 Dresden, Germany, and Department Chemie, Technische Universität München, 85747 Garching, Germany

Received November 21, 2008

Single crystals of CeAsSe were synthesized by a reaction of the elements using iodine as a mineralization agent at 900 °C. The crystal structure was established from single crystal X-ray diffraction data and obtained from a pseudomerohedrically twinned specimen (space group *Pnma*, $a = 5.7969(1)$ Å, $b = 5.7664(1)$ Å, and $c = 17.8196(6)$ Å; $Z = 8$). CeAsSe crystallizes in the GdPS type of structure and contains infinite cis−trans chains of arsenic atoms, packed between two-dimensional slabs of alternating Ce and Se atoms. The chemical composition of the investigated crystals was determined to be $CeAs_{1.01(1)}Se_{0.99(3)}$. High-resolution diffraction experiments with synchrotron radiation clearly evidence the orthorhombic metric. However, variations in composition or temperature profile in the synthesis procedure lead to vanishing distortion, that is, disappearance of reflection splitting and superstructure reflections, and thus to a tetragonal metric within the resolution of the synchrotron-based diffraction experiments. CeAsSe can be expressed as consisting of Ce^{3+}, As^{1-}, and Se^{2-} as an electronic precise Zintl-type compound. This interpretation is consistent with the results of X-ray absorption spectroscopy at the Ce−L_{III} edge and magnetic susceptibility data. The temperature dependence of a semiconductor was observed in electrical resistivity measurements.

Introduction

The physical properties of several ternary actinide metal compounds M—As—Se (M = U, Th) were intensively investigated, but little information on crystallographic details and relations to the chemical composition are available.[1] Phases near the equiatomic composition MAsSe crystallize in the ZrSiS type of structure (space group *P4/nmm*, alternatively designated as PbFCl type) and display a typical magnetic-field independent rise of the electrical resistivity toward lower temperatures (<20 K), which might be explained by a nonmagnetic Kondo effect.[2] Compounds with M = Zr and Hf like $ZrAs_{1.4}Se_{0.5}$[3−7] and $HfAs_{1.7}Se_{0.2}$[8] show similar behavior in electrical resistivity and were intensively investigated concerning their crystal structures and homogeneity ranges as well as chemical and physical properties. These Zr and Hf containing arsenide selenides also crystallize in the ZrSiS type of structure. The chemical composition in these compounds deviates from the ideal molar ratio of n(M):n(As):n(Se) = 1:1:1 because of vacancies within the arsenic layers and mixed occupation of nonmetal sites. Ternary rare-earth-metal arsenide selenides MAsSe with M = Pr, Nd, Sm, Gd−Tm, and Lu were reported to crystallize in the monoclinic CeAsS type of structure,[9] one of several known distortion variants of the ZrSiS type. There is no clear statement about the crystal structures of the corresponding La and Ce compounds. On the basis of X-ray powder diffraction (XRD) data, the authors supposed that these compounds are also isotypic with CeAsS. In the present paper, we report about the synthesis, crystal structure, metallographic investigations, magnetic and electric properties, and X-ray absorption spectroscopy (XAS) of CeAsSe. This system exemplifies further the crystallographic relationship among transition metal, rare earth, and actinide element compounds.

* To whom correspondence should be addressed. E-mail: rainer.niewa@mytum.de.
[†] Max-Planck-Institut für Chemische Physik fester Stoffe.
[‡] Technische Universität München.

(1) Schoenes, J.; Withers, R. L.; Hulliger, F. *J. Magn. Magn. Mater.* **2007**, *310*, 1778–1780.
(2) Henkie, Z.; Pietraszko, A.; Wojakowski, A.; Kępiński, L.; Cichorek, T. *J. Alloys Compd.* **2001**, *317*, 52–59.
(3) Schmidt, M.; Cichorek, T.; Niewa, R.; Schlechte, A.; Prots, Y.; Steglich, F.; Kniep, R. *J. Phys.: Condens. Matter* **2005**, *17*, 5481–5488.
(4) Schlechte, A.; Schmidt, M.; Cichorek, T.; Simon, P.; Prots, Y.; Doert, T.; Niewa, R.; Steglich, F.; Kniep, R. *Z. Kristallogr. Suppl.* **2005**, *22*, 115.
(5) Schlechte, A.; Niewa, R.; Cichorek, T.; Prots, Y.; Schmidt, M.; Ramlau, R.; Kniep, R. *Z. Anorg. Allg. Chem.* **2006**, *623*, 2107.

10.1021/ic802246g CCC: $40.75
Published on Web 01/28/2009

Experimental Section

Crystals of CeAsSe were synthesized by a reaction of the elements (Ce, Ames, 99.99+ wt %, ingots; As, Chempur, 99.999 wt %, pieces; and Se, Chempur, 99.999 wt %, pellets) in a molar ratio of n(Ce):n(As):n(Se) = 1:1.05:0.95 by using iodine (12 mg/cm^3 of ampule volume) as a mineralization agent at 900 °C. The reaction was carried out in a fused silica ampule with a small plugged glassy carbon crucible (diameter ≈ 1.5 cm, length ≈ 4 cm) to avoid side reactions of the rare-earth metal with the ampule material. For best results, after one month of heat treatment, the sample was allowed to cool down to 400 °C and kept at this temperature for three further days. Afterward, the ampule was quenched in water. The sample was subsequently washed with acetone, dried in air, and then stored in an argon-filled glovebox ($p(O_2/H_2O) \leq 1$ ppm, purification by molecular sieves and copper catalyst). The product predominantly consists of a microcrystalline powder matrix with a small number of plate-like crystals with edge dimensions up to 500 μm. Further samples were obtained in similar ways from different initial ratios of the elements and various temperature profiles.

Powdered samples were characterized by XRD Guinier diagrams (Huber Image Plate Camera G670, Cu Kα_1 radiation, $5° \leq 2\theta \leq 100°$, using LaB_6, a = 4.15692 Å, as internal standard). Selected samples were investigated on the high-resolution powder diffraction beamline ID31 (ESRF, Grenoble) by using synchrotron radiation (λ = 0.39987 Å, glass capillaries with diameter of 0.3 mm). Lattice parameters were refined with the program package WinCSD.[10] Single crystal XRD intensity data were collected with a four axis diffractometer (Rigaku AFC 7 equipped with Mercury CCD area detector) by using Mo Kα radiation.

Selected single crystals were investigated by electron probe microanalysis (EDXS, PHILIPS XL 30). The chemical composition was quantified either with wavelength-dispersive X-ray spectroscopy (WDXS, CAMECA SX 100, $CeAl_2$ as well as elemental As and Se as standards) or by chemical analyses (CA), applying the inductively coupled plasma optical emission spectrometry (ICP-OES, Varian, VISTA RL) method. No foreign impurity components were observed in any analysis.

The magnetic susceptibility was measured on powders in a SQUID magnetometer (MPMS XL7, Quantum Design) by applying external fields between 100 Oe and 70 kOe in the temperature range of 1.8−400 K. The measurement of the electrical resistivity was carried out on pressed powder samples in the temperature range of 3.8−320 K.[11] The heat capacity measurements were performed with a relaxation-type calorimeter (PPMS, Quantum Design) in magnetic fields up to 90 kOe between 1.8 and 100 K.

XAS data were taken on powdered samples with CeO_2 as an energy reference on the Ce−L_{III} edge at about 5723 eV. The data were collected at beamline E4 located at the DORIS III storage ring in the HASYLAB at DESY in Hamburg (Germany). For these measurements, powdered samples were mixed with B_4C in a volume ratio of 1:3 and a small amount of low-melting paraffin was added. This mixture was warmed to about 60 °C to form a sticky mass and loaded in a steel frame with polyimide windows.

Results and Discussion

Crystal Structure Determination. The first experiments to synthesize single crystals of CeAsSe were carried out by direct reaction of the elements in the molar ratio n(Ce):n(As):n(Se) = 1:1:1 at 900 °C in glassy carbon crucibles for one month and subsequent quenching to ambient temperature. The microcrystalline powder product contained a large number of small crystals with platelet shapes. The chemical composition of the crystals was determined to be $CeAs_{0.94(2)}Se_{1.01(5)}$ from WDXS. The composition was confirmed by CA on bulk powder samples, which resulted in $CeAs_{0.87(1)}Se_{1.03(1)}$. The XRD powder pattern of such samples showed a pronounced set of the reflections, which were indexed on the basis of a tetragonal unit cell compatible with the ZrSiS type of structure ($a \approx 4.09$ Å, $c \approx 8.90$ Å). Nevertheless, careful examination of the powder diagram indicated that the full width at half-maximum of most reflections was significantly larger compared to those of the $h0l$ and $00l$ reflections, indicating an orthorhombic distortion of the original tetragonal unit cell along the ⟨110⟩ direction ($a' \approx \sqrt{2}a$, $b' \approx \sqrt{2}a$). Furthermore, additional reflections with very low intensity were present, leading to an enlarged unit cell in [001] ($c' = 2c$). For intensity data collection by applying X-ray single-crystal diffraction technique, a well-formed specimen was selected (crystal **I**). Analysis of the obtained data set clearly indicated the unit cell dimensions of $a \approx 5.78$ Å, $b \approx 5.78$ Å, and $c \approx 17.79$ Å expected from XRD data. Even though the analysis of the reflection intensities revealed the tetragonal *Laue* symmetry 4/*mmm* (R(int) = 0.031), our attempts to find a reasonable structure solution in any tetragonal space group failed. Therefore, taking into account our observations on the X-ray powder diagrams, we reduced the symmetry to orthorhombic (*mmm*). However, as a result of the presence of numerous reflections violating the extinction conditions for the presence of glide planes, the assignment of the correct space group was still difficult. This is caused by the tendency of CeAsSe to form twinned crystal individuals. The latter fact was confirmed by microscopic investigations with polarized light shown in Figure 1a,b. The images taken on crystals prepared at 900 °C and quenched to ambient temperature as described above clearly evidence small and interpenetrating twinning domains.

To establish a valid crystal structure model, we first solved and refined a subcell model in the smaller tetragonal unit cell (a = 4.0908 Å, c = 8.896 Å) in *P*4/*nmm* from only the strongest reflections with integer indices in this setting. The structure solution resulted in an atomic arrangement of the ZrSiS type with Ce and Se atoms in 2*c* sites and As in 8*i* with an occupancy factor of 25%. The structural result is depicted in Figure 2. Selected crystallographic data are summarized in Tables 1 and 2. This structural model, namely, the location of the As atoms, has large similarities with the

(6) Cichorek, T.; Gnida, D.; Niewa, R.; Schlechte, A.; Schmidt, M.; Prots, Yu.; Ramlau, R.; Henkie, Z.; Kniep, R.; Steglich, F. *J. Low Temp. Phys.* **2007**, *147*, 309–319.
(7) Schlechte, A.; Niewa, R.; Schmidt, M.; Auffermann, G.; Prots, Yu.; Schnelle, W.; Gnida, D.; Cichorek, T.; Steglich, F.; Kniep, R. *Sci. Technol. Adv. Mater.* **2007**, *8*, 341–346.
(8) Schlechte, A.; Niewa, R.; Schmidt, M.; Borrmann, H.; Auffermann, G.; Kniep, R. *Z. Kristallogr. New Cryst. Struct.* **2007**, *222*, 369–370.
(9) Schmelczer, R.; Schwarzenbach, D. *Z. Naturforsch.* **1981**, *36b*, 463–469.
(10) Akselrud, L. G.; Zavalii, P. Y.; Grin, Y. N.; Pecharsky, V. K.; Baumgartner, B.; Wölfel, E. *Mater. Sci. Forum* **1993**, *133−136*, 335–340.
(11) Schnelle, W.; Niewa, R.; Wagner, F. R. *J. Magn. Magn. Mater.* **2004**, *828*, 272–276.

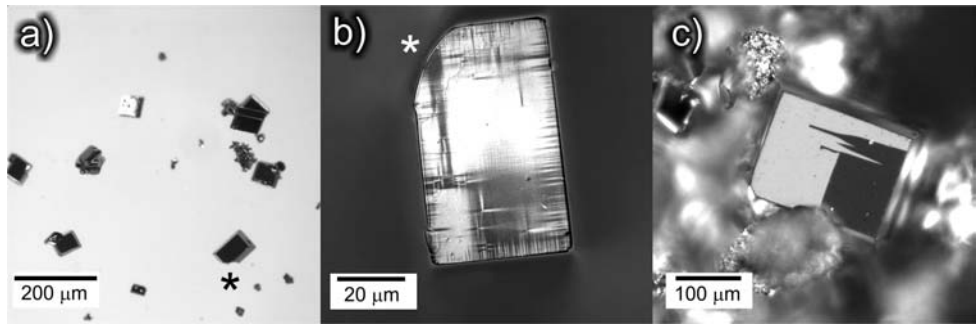

Figure 1. Light microscopic images of different crystals in polarized light evidencing twinning domains: (a) plate-shaped crystals, synthesized at 900 °C and quenched to ambient temperature, (b) enlarged image of the crystal marked by asterisk in (a), which evidences badly conditioned twinning domains in polarized light, and (c) crystal synthesized at 900 °C with additional annealing at 400 °C prior quenching to ambient temperatures. Well-defined twinning domains are visible in polarized light (dark and light regions).

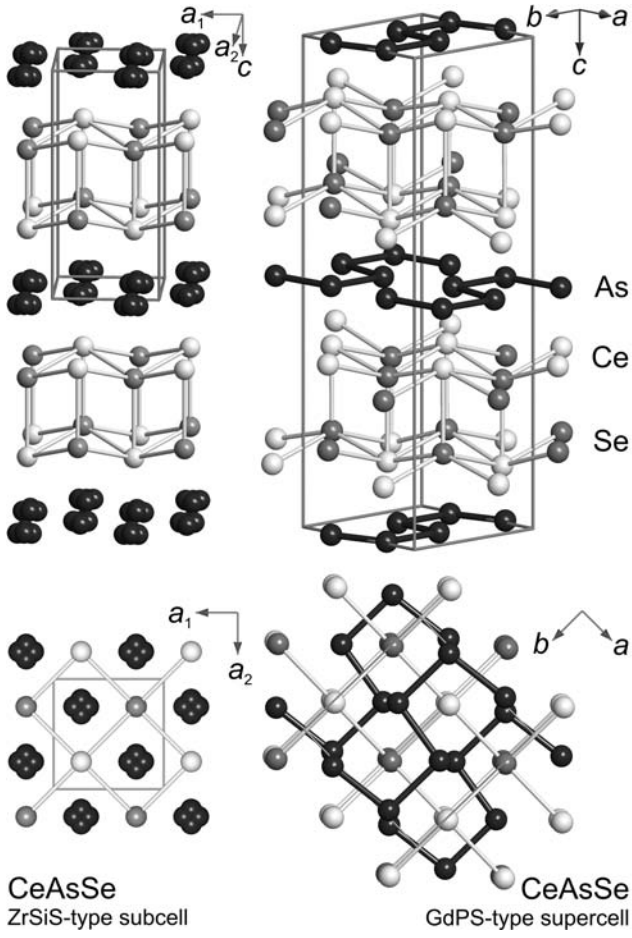

Figure 2. Crystal structure of the split model (left), which represents the ZrSiS-type subcell (space group *P*4/*nmm*) and the orthorhombic model (right) in the GdPS type of structure (space group *Pnma*).

$HfCuSi_2$ type subcell recently obtained during investigations of the crystal structure of $CeAgAs_2$.[12] The crystal structures of ZrSiS and $HfCuSi_2$ types (both in space group *P*4/*nmm*) are closely related, and one can assume the latter is a filled variant of the first one. In analogy to the previous investigation, we turned back to the large supercell with $a = 5.7950(2)$ Å, $b = 5.7755(3)$ Å, and $c = 17.7926(9)$ Å and developed a structural model with infinite cis−trans chains of As atoms and reasonable interatomic As−As distances, that is, the GdPS structure type (space group *Pnma*). In refinements of this model, the twinning law 0 1 0 $\bar{1}$ 0 0 0 0 1 was implemented. The refinement resulted in the reasonable low residuals of $R1 = 0.041$ and $wR2 = 0.114$; however, the displacement parameters of As atoms were large, and the values of U_{11} and U_{22} were about 3 times larger than U_{33}; that is, our refinements still described an averaged dislocation of As atoms within the (001) plane. We repeatedly analyzed the XRD powder diagram and came to the conclusion that the sample suffers from disorder, because no clear splitting of the reflections responsible for the orthorhombic distortion (all reflections with the exception of *h*0*l* and 00*l*, in the tetragonal setting) was observed. The degree of the splitting of these reflections is connected with the degree of the orthorhombic distortion of the tetragonal subcell, namely, with the degree of the ordering of As atoms within the cis−trans chains. A possible substitution of some As by Se and vice versa cannot be excluded from the available XRD data because of the nearly identical atomic form factors of As and Se—this fact applies throughout the paper; however, particularly for compositions close to CeAsSe from a chemical point of view, we expect only minor substitution.

A series of new syntheses was performed to optimize crystal growth and to obtain samples with a completely ordered crystal structure. As a quantitative criterion of the order, we used the degree of splitting of the above-mentioned reflections in XRD powder patterns. During the progress of these experiments, the molar ratio of the starting components *n*(Ce), *n*(As), and *n*(Se) was varied in the range from 1:1.2:0.8 to 1:0.8:1.2. The optimum was found for a molar ratio of *n*(Ce):*n*(As):*n*(Se) = 1:1.05:0.95. Additionally, an annealing step at 400 °C for several days was introduced directly after the synthesis at 900 °C. As a result of this treatment, well-defined twinning domains with very sharp domain boundaries emerge in light microscopic images in polarized light (Figure 1c). In the XRD powder pattern of the samples treated in this way, a clearly recognizable splitting of the reflections could be observed (Figure 3). This proves that a well-defined distortion of the tetragonal metric of the ZrSiS type of structure to an orthorhombic unit cell can be obtained with proper heat treatment. Furthermore, superstructure reflections with $l \neq 2n$ were now clearly

(12) Demchyna, R.; Jemetio, J. P. F.; Prots, Y.; Doert, T.; Akselrud, L. G.; Schnelle, W.; Kuz'ma, Y.; Grin, Y. *Z. Anorg. Allg. Chem.* **2004**, *630*, 635–641.

Table 1. Crystal Data and Experimental Details for Two Crystal Specimens of CeAsSe

specimen	crystal **I**		crystal **II**	
crystal size, mm^3	0.040 × 0.040 × 0.065		0.050 × 0.050 × 0.080	
composition[a]	$CeAs_{0.96(2)}Se_{1.03(5)}$		$CeAs_{1.01(1)}Se_{0.99(3)}$	
diffractometer, detector	ACF 7, Mercury CCD			
radiation, λ	Mo Kα, 0.71073 Å			
scans, step	φ, ω, 0.6°			
2θ range up to	64°		69°	
	subcell	**supercell**	**subcell**	**supercell**
structure type	ZrSiS	GdPS	ZrSiS	GdPS
space group	*P*4/*nmm*	*Pnma*	*P*4/*nmm*	*Pnma*
cell parameters[b]				
a, Å	4.0908(2)	5.7950(2)	4.0882(1)	5.7969(1)
b, Å		5.7755(3)		5.7664(1)
c, Å	8.896(1)	17.7926(9)	8.9098(6)	17.8196(6)
V, Å^3	148.87(1)	595.50(4)	148.91(1)	595.66(2)
Z	2	8	2	8
hkl ranges	$-5 \le h \le 5$	$-8 \le h \le 6$	$-6 \le h \le 6$	$-7 \le h \le 9$
	$-5 \le k \le 5$	$-8 \le k \le 8$	$-6 \le k \le 3$	$-9 \le k \le 6$
	$-11 \le l \le 12$	$-22 \le l \le 25$	$-13 \le l \le 12$	$-27 \le l \le 24$
N (*hkl*) measured	1404	5139	1413	5807
N (*hkl*) unique	168	1066	217	1404
R(int)[c]	0.023	0.027	0.042	0.049
N (*hkl*) observed	165	894	213	1175
refined parameters	11	36	11	36
w*R*2[c]	0.114	0.091	0.041	0.058
*R*1[c]	0.041	0.042	0.018	0.029
twin domains ratio		0.526(4):0.474		0.537(2):0.463
residual peaks (e Å^{-3})	1.11, −1.07	2.95, −1.68	1.15, −1.66	1.75, −1.76

[a] Obtained from WDXS analyses. [b] Obtained from XRD powder data (LaB_6, $a = 4.15692$ Å as internal standard). Relation between subcell and supercell lattices: a(subcell) $= {}^1/_2(a$(supercell) $+ b$(supercell))$/\sqrt{2}$; c(subcell) $= {}^1/_2 c$(supercell); transformation matrix (a, b, c) subcell $= ({}^1/_2\ {}^1/_2\ 0\ -{}^1/_2\ {}^1/_2\ 0\ 0\ 0\ {}^1/_2)$ (a, b, c) supercell). [c] The residuals are defined as follows: $R(\text{int}) = \sum(F - F(\text{mean}))/\sum(F)$, $R1 = \sum(|F_o| - |F_c|)/\sum|F_o|$, $wR2 = \{\sum[w(F - F)^2/\sum[w(F)^2]\}^{1/2}$.

Table 2. Atomic Coordinates and Displacement Parameters of CeAsSe (in 10^2 Å^2)[a]

atom	site	*x*	*y*	*z*	U_{11}	U_{22}	U_{33}	U_{23}	U_{13}	U_{12}	$U_{eq/iso}$
					Crystal **I**						
					Subcell (split-model, *P*4/*nmm*)						
Ce	2*c*	1/4	1/4	0.71832(5)	1.04(2)	U_{11}	1.34(3)	0	0	0	1.14(2)
Se	2*c*	1/4	1/4	0.37104(8)	0.92(3)	U_{11}	1.02(4)	0	0	0	0.96(2)
As[b]	8*i*	3/4	0.3178(4)	0.0031(3)							0.89(4)
					Supercell (*Pnma*)						
Ce1	4*c*	0.0087(1)	1/4	0.35685(4)	0.73(9)	0.98(8)	1.00(5)	0	−0.06(2)	0	0.80(2)
Ce2	4*c*	0.4917(1)	1/4	0.63843(4)	0.70(9)	1.00(9)	1.23(5)	0	0.11(2)	0	0.98(2)
Se1	4*c*	0.0070(1)	1/4	0.18381(6)	0.7(2)	0.8(2)	0.80(5)	0	−0.03(4)	0	0.78(3)
Se2	4*c*	0.4925(2)	1/4	0.81278(6)	0.6(2)	0.8(2)	0.96(6)	0	0.00(4)	0	0.82(3)
As[c]	8*d*	0.2786(2)	0.0253(2)	0.00115(6)	2.66(6)	2.57(6)	0.98(5)	0.20(7)	0.33(3)	0.32(3)	2.07(4)
					Crystal **II**						
					Subcell (split-model, *P*4/*nmm*)						
Ce	2*c*	1/4	1/4	0.71906(4)	1.10(2)	U_{11}	1.32(2)	0	0	0	1.18(2)
Se	2*c*	1/4	1/4	0.37159(7)	0.93(2)	U_{11}	0.99(3)	0	0	0	0.95(2)
As[b]	8*i*	3/4	0.3163(3)	0.0034(3)							0.87(3)
					Supercell (*Pnma*)						
Ce1	4*c*	0.01173(7)	1/4	0.35625(2)	0.39(3)	1.35(4)	0.83(3)	0	0.02(2)	0	0.86(1)
Ce2	4*c*	0.48895(7)	1/4	0.63705(2)	0.50(3)	1.23(4)	1.06(3)	0	0.02(2)	0	0.93(1)
Se1	4*c*	0.0091(1)	1/4	0.18328(4)	0.45(6)	1.17(7)	0.82(3)	0	0.02(3)	0	0.81(2)
Se2	4*c*	0.4902(1)	1/4	0.81177(4)	0.44(6)	0.99(7)	0.76(3)	0	0.00(3)	0	0.73(2)
As	8*d*	0.28356(9)	0.03081(9)	0.00174(3)	0.98(3)	1.15(3)	0.83(2)	0.05(3)	0.05(2)	−0.01(2)	1.05(1)

[a] The structure model of CeAsSe (supercell) was standardized by using the program STRUCTURE TIDY.[24,25] [b] Occupancy fixed at 0.25. [c] Occupancy 0.972(5).

visible. The strongest superstructure reflection (113) increased from 1 to 3% of the intensity of the most intense reflection (116) in comparison with the initially described experiment. The chemical composition of the crystals was determined with WDXS to $CeAs_{1.01(1)}Se_{0.99(3)} \equiv$ CeAsSe. A single crystal XRD study (crystal **II**) resulted in significantly lower residuals and revealed reasonable anisotropic displacement parameters of the As atoms. For comparison, the results of both structure refinements are listed in Tables 1 and 2. For the structure description and the following discussion, we exclusively used the results obtained from crystal **II**.

Crystal Structure Description. CeAsSe crystallizes in the GdPS structure type, an orthorhombic derivative of the tetragonal ZrSiS type of structure. For comparison, both structure types are represented in Figure 2 by using the atomic parameters obtained during the structure refinements of the sub- and supercells of CeAsSe (Table 2). While Ce and Se atoms in both structure models produce corrugated

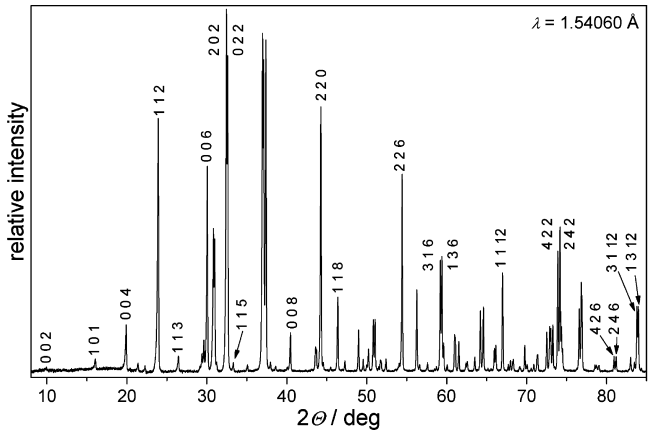

Figure 3. XRD powder pattern (Cu $K\alpha_1$ radiation) of a microcrystalline sample $CeAs_{1.01(1)}Se_{0.99(3)}$, which shows the largest observed reflection splitting. Miller indices of selected reflections are given according to the orthorhombic supercell.

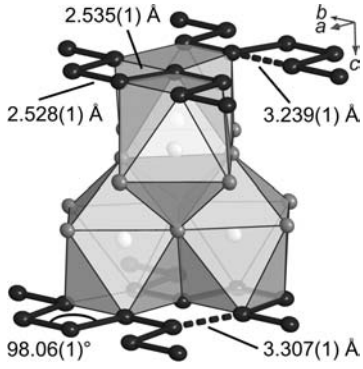

Figure 4. Arrangement of slightly distorted monocapped square antiprisms with cerium as the central atom (white spheres). Black spheres in cis−trans chains represent As atoms and light gray spheres embody Se atoms. All ellipsoids are shown with 99% probability level.

slabs perpendicular to [001] of virtually identical arrangement, the positions of the arsenic atoms vary slightly. In the ideal ZrSiS type of structure, the As atoms are located on a four-fold axis, that is, occupying a special site 2*a* (3/4, 1/4, 0). In the case of the description of CeAsSe in the tetragonal subcell, this site is splitted into an eight-fold position at site 8*i* (3/4, *y*, *z*) with an occupation of 25%. The orthorhombic GdPS type of structure allows a description of the arrangement of As atoms in an ordered manner, leading to infinite cis−trans As chains with a bond angle of 98.06(1)°. The alternating distances of 2.535(1) Å and 2.528(1) Å within the chains agree very well with As−As contacts of 2.52 Å in the rhombohedral modification of arsenic[13] and can be considered as covalent two electron−two center bonds. The distances between nonbonded atoms within the chains and the shortest interchain contacts are 3.239(1) Å and 3.307(1) Å, respectively (Figure 4). The coordination environment of cerium is formed by nine atoms located in the apexes of a distorted tetragonal antiprism (4As + 4Se) capped by one atom (1Se). The Ce−As and Ce−Se distances cover the ranges from 3.1227(6) to 3.3063(6) Å and from 2.968(9) to 3.1134(8) Å, respectively. The relation between the space groups of the subcell and the supercell of the CeAsSe

(13) Schiferl, D.; Barrett, C. S. *J. Appl. Crystallogr.* **1969**, *2*, 30–36.

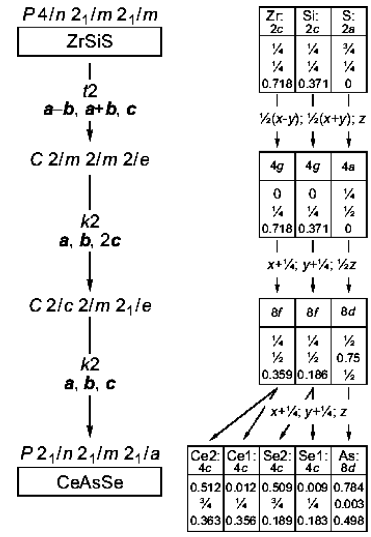

Figure 5. Group−subgroup scheme[14] for the tetragonal subcell (ZrSiS type) and the orthorhombic supercell (GdPS type) of CeAsSe. The left part represents the symmetry reduction (translationsgleiche (*t*) or klassengleiche (*k*), both of index 2) and unit cell transformation starting from the space group of the subcell: *P*4/*nmm* (No. 129) → *Cmma* (*Cmme*, No. 67) → *Ccma* (*Ccme*, nonstandard setting of *Cmca* = *Cmce*, No. 64) → *Pnma* (No. 62). The relationship between the atomic coordinates is shown on the right.

structure by using group−subgroup formalism is presented in Figure 5.[14]

The distortion of the square-planar arsenic layers, described by the subcell model (ZrSiS type) of the cis−trans chains in the final structure model, is one of four possibilities for the formation of arsenic polyanions discussed in literature.[15,16] Zig-zag chains (As^{1-}) were found in CeAsS,[17] GdAsSe,[9] and $PrAgAs_2$,[18] and $[As—As]^{2-}$ dumbbells were observed in NdAsSe[9] beside a hypothetical four-ring formation. In this context, one should emphasize that only the model containing cis−trans chains requires an increased lattice parameter *a* of the subcell by a factor of $\sqrt{2}$, that is, the deformation of the unit cell along ⟨110⟩. Distortions of square-planar layers were studied and discussed by Tremel and Hoffmann[15] with focus on the electronic structures. According to their results, distortions to chains or dumbbells are preferred if the concentration per layer atom exceeds six electrons. This is the case in CeAsSe, based on the postulate that cerium can be described as Ce^{3+} (see Physical Properties section below), As^{1-} is present within the infinite chains, and isolated selenium Se^{2-} ions exist. A substitution of those components by elements with smaller numbers of valence electrons (i.e., Si for As) should lead to compounds which do not show any signs of distortion, like CeSiFe.[19]

Homogeneity Ranges and Degree of Order. As described in the previous sections, we have performed various experiments to optimize the synthesis conditions of CeAsSe. In the following, we present selected results of these

(14) Bärnighausen, H. *MATCH* **1980**, *9*, 139–175.
(15) Tremel, W.; Hoffmann, R. *J. Am. Chem. Soc.* **1987**, *109*, 124–140.
(16) Hulliger, F.; Schmelczer, R.; Schwarzenbach, D. *J. Solid State Chem.* **1977**, *21*, 371–374.
(17) Céolin, R.; Khodadad, P.; Sfez, G. *J. Magn. Magn. Mater.* **1972**, *274*, 1731–1734.
(18) Eschen, M.; Jeitschko, W. *Z. Naturforsch.* **2003**, *58b*, 399–409.
(19) Bodak, O. I.; Hladyshevskii, E. I.; Kripyakevich, P. I. *Zh. Strukt. Khim.* **1970**, *11*, 305–310.

Table 3. Dependence of the Chemical Composition (Determined by CA or WDXS) on the Lattice Metric

			lattice parameters		
powder pattern[a]	chemical composition[b]	indexed in space group	*a*, Å	*b*, Å	*c*, Å
(a)	$CeAs_{0.991(4)}Se_{0.853(5)}$	*P4/nmm*	4.10128(2)	*a*	8.92197(7)
(b)	$CeAs_{1.01(1)}Se_{0.99(3)}$	*Pnma*	5.7969(1)	5.7664(1)	17.8196(6)
(c)	$CeAs_{0.94(2)}Se_{1.01(5)}$	*Pnma*	5.7950(2)	5.7755(3)	17.7926(9)
(d)	$CeAs_{0.817(8)}Se_{1.108(9)}$	*P4/nmm*	4.10445(1)	*a*	8.85850(5)

[a] See Figure 6. [b] (a, d) CA; (b, c) WDXS.

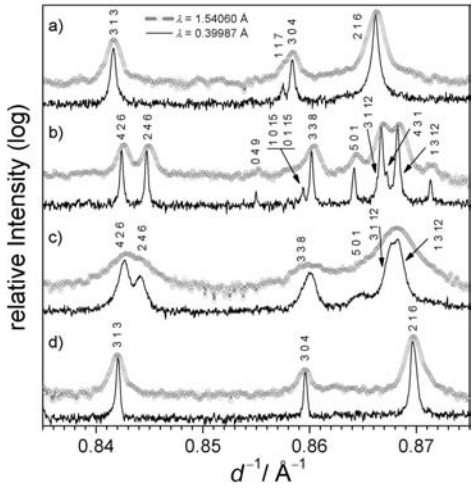

Figure 6. X-ray (gray circles, Cu $K\alpha_1$ radiation, $\lambda = 1.54060$ Å) and synchrotron powder (solid black line, $\lambda = 0.39987$ Å) diffraction patterns of $CeAs_xSe_y$ compounds with slightly different chemical compositions. All intensities are depicted in logarithmic scale: (a) the tetragonal indexed pattern of $CeAs_{0.991(4)}Se_{0.853(5)}$ with absence of any reflection splitting and superstructure reflections, (b) the orthorhombic indexed pattern of $CeAs_{1.01(1)}Se_{0.99(3)}$ (crystal **II**) with clearly splitted reflections, (c) the diffraction pattern of $CeAs_{0.94(2)}Se_{1.01(5)}$ (crystal **I**) containing weakly splitted reflections, and (d) the diffraction pattern of $CeAs_{0.817(8)}Se_{1.108(9)}$. Miller indices are given on the basis of the subcell for patterns (a) and (d) and on the basis of the supercell for patterns (b) and (c). Correlations with the chemical compositions from CA and WDXS are listed in Table 3.

investigations. Slight changes in the molar starting ratio *n*(Ce):*n*(As):*n*(Se) in the synthesis have a significant effect on the degree of order in the As containing slabs. We generalize four variants of $CeAs_xSe_y$ with different chemical compositions close to CeAsSe (Table 3).

The chemical composition of the crystals obtained with the starting molar ratio *n*(Ce):*n*(As):*n*(Se) = 1:1.15:0.85 was determined to be $CeAs_{0.991(4)}Se_{0.853(5)}$. This is the compound with the highest observed selenium deficiency. In the XRD powder patterns, both reflection splitting and superstructure reflections were absent, and the data can be fully indexed on the basis of the tetragonal subcell. This finding was corroborated by high-resolution synchrotron powder diffraction data, which show no indication of any reflection broadening or superstructure reflections (black solid line in Figure 6a).

For the starting ratio *n*(Ce):*n*(As):*n*(Se) = 1:1.05:0.95, the reaction product must be described as CeAsSe (1:1:1) within the errors of the composition determination. This is the compound described above in detail (crystal **II**), which shows the large reflection splitting and clear superstructure reflections in XRD powder diagrams. By reducing the initial amount of arsenic from 1.05 to 1, the composition $CeAs_{0.99(1)}Se_{0.95(1)}$ was observed, a compound with similar features in the XRD powder pattern to CeAsSe (shown in Figure 6b). Apparently, phases within a composition range from CeAsSe to $CeAs_{0.99(1)}Se_{0.95(1)}$ are best described in the orthorhombic space group *Pnma* (supercell).

The XRD powder pattern presented in Figure 6c was collected from a sample synthesized with a starting molar ratio of *n*(Ce):*n*(As):*n*(Se) = 1:1:1. Very weak superstructure reflections and hardly recognizable reflection splitting (line broadening) in XRD powder patterns lead to orthorhombic lattice parameters of $a = 5.7950(2)$ Å, $b = 5.7755(3)$ Å, and $c = 17.7926(9)$ Å. Determination of the chemical composition applying WDXS results in $CeAs_{0.94(2)}Se_{1.01(5)}$. The single crystal XRD investigation on a selected single crystal is described above (crystal **I**). Refinements of the data confirm the vacancies in the arsenic layer; the occupation factor of arsenic converged to 0.972(5).

A further reduction of the arsenic content in the starting ratio to *n*(Ce):*n*(As):*n*(Se) = 1:0.9:1.1 leads to a compound which shows tetragonal metric in XRD powder patterns; neither reflection splitting nor superstructure reflections were observed (Figure 6d). The diffraction pattern was indexed with a tetragonal unit cell with $a = 4.10445(1)$ Å and $c = 8.85850(5)$ Å. The chemical composition of this compound was determined to be $CeAs_{0.817(8)}Se_{1.108(9)}$ by CA. Generally, the lattice parameter *c* decreases systematically with decreasing arsenic (*x*) and increasing selenium (*y*) amount in $CeAs_xSe_y$.

Physical Properties

Electrical Resistivity. The electrical resistivity $\rho(T)$ of a cold-pressed powder sample of the composition $CeAs_{0.87(1)}Se_{1.03(1)}$ is shown in Figure 7. The order of magnitude and the activated temperature dependence of the resistivity prove that the compound behaves as a semiconductor, in agreement with the aforementioned considerations. From the temperature dependence of $\rho(T)$ (between 250 K and the temperature of the highest reliably measured resistance), a minimum estimate for the fundamental band gap of $\Delta E_g \approx 0.25$ eV can be obtained.

Magnetic Susceptibility. The magnetic susceptibility $\chi(T)$ of a batch of selected single crystals, which have a composition of $CeAs_{0.94(2)}Se_{1.01(5)}$, is shown for a field of $H = 10$ kOe in Figure 8. At high temperatures, $\chi(T)$ may be described by a Curie−Weiss law, while at lower temperatures, deviations due to the splitting of the crystal electric field (CEF) ground-state multiplet are dominant. The effective magnetic moment of $\mu_{eff} = 2.54\ \mu_B$ (accidentally, just the free-ion value) obtained from the nonlinear Curie−Weiss fit in the temperature range 80−400 K is consistent with the $^2F_{5/2}$ ground multiplet state of the $4f^1$ configuration of Ce^{3+}. The

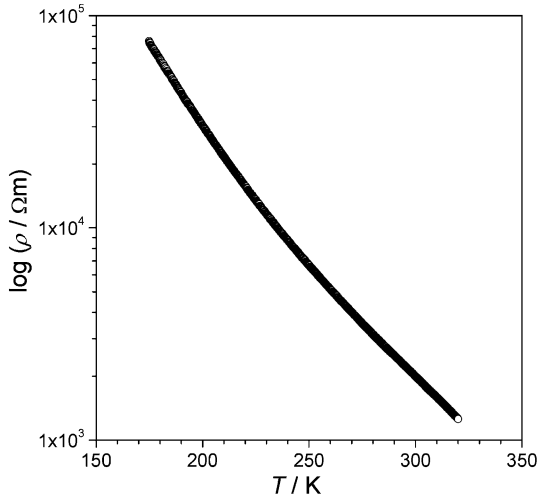

Figure 7. Electrical resistivity vs temperature of $CeAs_{0.87}Se_{1.03}$. The semiconducting characteristic down to 170 K is visible; below that temperature, the electrical resistance exceeded the range of the experimental setup.

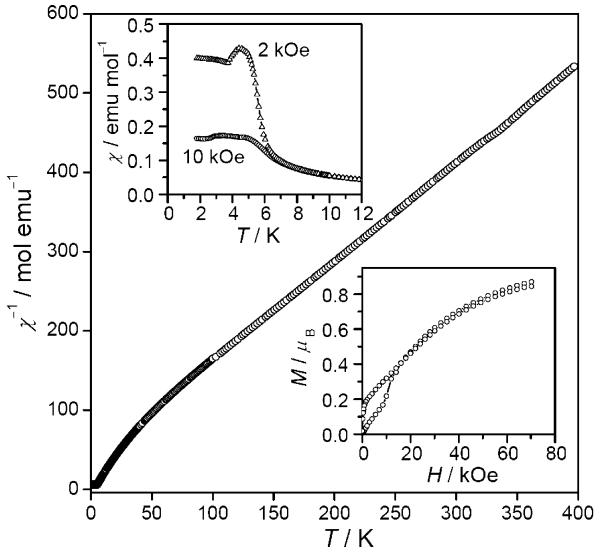

Figure 8. Reciprocal magnetic susceptibility, $1/\chi$, of $CeAs_{0.94}Se_{1.01}$ as a function of temperature for $H = 10$ kOe. The upper inset shows $\chi(T)$ for temperatures around the magnetic ordering at $T_N \approx 6$ K. The lower inset displays an isothermal magnetization curve at $T = 1.8$ K.

paramagnetic Weiss temperature from this fit results in $\theta_p = -32.7$ K and is merely due to the CEF splitting.

Magnetic interactions are present, since at $T_N \approx 5.3$ K a complex magnetic ordering of the Ce moments is visible. For low fields ($\leq$100 Oe) this transition shows, both in field-cooling and zero-field cooling data, an atypically strong rise of $\chi(T)$ with decreasing T, a sharp peak at T_N, and a strong decrease immediately below that temperature. In higher fields, the rise of $\chi(T)$ at around T_N remains and broadens with increasing field; however, the decrease of $\chi(T)$ shifts to lower temperature with increasing field (e.g., to 2.8 K at $H = 10$ kOe). This complex behavior might be interpreted by the existence of an intermediate magnetic ordering structure with a weak ferromagnetic component ($\mu_{fm} \approx 0.1$ μ_B at $H = 100$ Oe) which gives place to another, predominantly antiferromagnetically ordered structure at a lower temperature. An isothermal magnetization measurement at

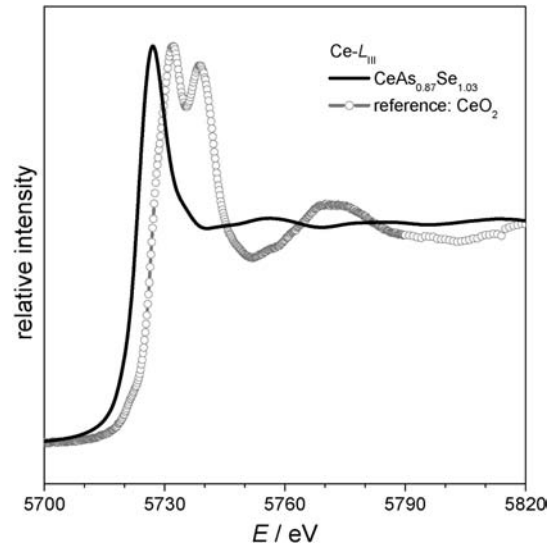

Figure 9. X-ray absorption spectrum of $CeAs_{0.87(1)}Se_{1.03(1)}$ at the Ce$-L_{III}$ absorption edge, compared to the reference compound CeO_2.

$T = 1.8$ K (inset in Figure 8) reveals a slightly curved increase of M with H up to about 8 kOe, a broad metamagnetic transition beginning at this field, and above 16 kOe again a regular increase of M which tends toward a saturation. At $H = 70$ kOe, a value of 0.87 μ_B is attained. When reducing the field, it is found that the metamagnetic transition is not reversible down to $H = 0$. Instead, a residual magnetization of 0.9 μ_B remains.

XAS. For independent information on the electronic state of cerium, we measured XAS spectra on the Ce$-L_{III}$ threshold. It is well-known that Ce($4f^1$) compounds show a single peak structure in the L_{III} XAS spectra, whereas the spectrum of Ce($4f^0$) compound exhibits two maxima. This is attributed to covalency effects in the sense of a partial back-donation of charge from the formally closed shell anions.[20] Figure 9 shows the Ce$-L_{III}$ edge of $CeAs_{0.87(1)}Se_{1.03(1)}$ together with the spectrum of CeO_2 as a reference. It can be seen not only that the spectrum of $CeAs_{0.87(1)}Se_{1.03(1)}$ displays one maximum but also that the white line is clearly shifted by 4.2(1) eV toward lower energies as compared to the onset of the double maximum signal of CeO_2, both facts indicating a pure Ce($4f^1$) state in the arsenide selenide. The comparably small shift in energy between the Ce($4f^1$) and the Ce($4f^0$) compound is attributed to the lower electronegativity of As and Se as compared to O.[21,22]

Heat Capacity. Preliminary measurements of heat capacity in the fields of 0, 60 kOe, and 90 kOe were performed on a sample with a similar composition to that used in susceptibility measurements (Figure 10). The specific heat capacity $C_p(T)$ for $H = 0$ shows a sharp λ peak at 5.3 K, in agreement with the observations in the magnetic susceptibility data. By subtraction of the specific heat of LaAsSe, the magnetic contribution $C_{mag}(T)$ was obtained. The integrated magnetic entropy $S_{mag}(T)$ in the inset of Figure 10 shows

(20) Kaindl, G.; Wertheim, G. K.; Schmiester, G.; Sampathkumaran, E. V. *Phys. Rev. Lett.* **1987**, *58*, 606–609.
(21) Hu, Z.; Kaindl, G.; Meyer, G. *J. Alloys Compd.* **1997**, *246*, 186–192.
(22) Niewa, R.; Hu, Z.; Kniep, R. *Eur. J. Inorg. Chem.* **2003**, 1632–1634.

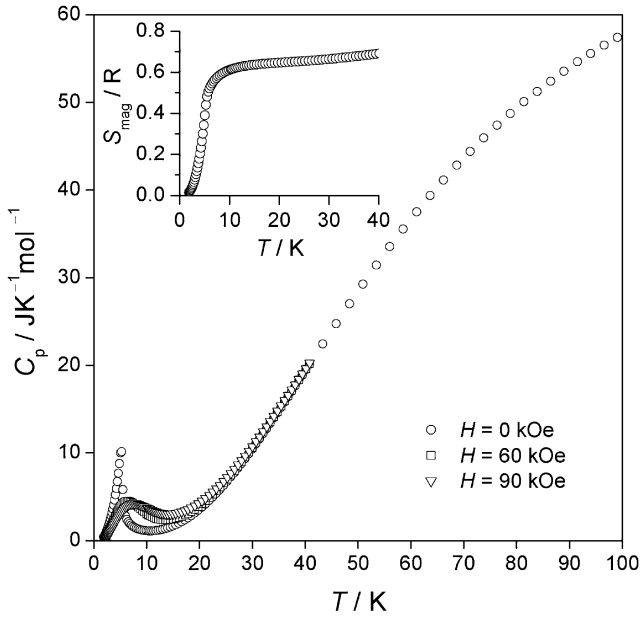

Figure 10. Temperature dependence of C_p for $CeAs_{0.958(8)}Se_{1.023(7)}$ in three different magnetic fields. The inset shows the magnetic entropy against temperature.

values around 0.64 R ($R = N_A k_B$) at temperatures some Kelvin above the ordering transition, indicating that the CEF ground state in $CeAs_{0.958(8)}Se_{1.023(7)}$ (expected entropy R ln $2 \approx 0.69\ R$) is a doublet. Since no significant reduction of magnetic entropy of the ground state is observed, the (magnetic) Kondo effect should be weak in $CeAs_{0.958(8)}Se_{1.023(7)}$. Ce $4f^1$ is a Kramers ion, and the Ce site symmetry is lower than cubic. Thus, two further CEF doublets are expected at some energy splitting from the ground doublet. From the analysis of the Schottky anomaly, the energy of the first exited doublet is large (>150 K). For the two measurements in rather high magnetic fields, the magnetic ordering is already suppressed, and the Schottky peak of the ground Kramers doublet, which is now split by the Zeeman effect, is observed.

Both magnetic susceptibility and specific heat results indicate that CeAsSe has a complex magnetic phase diagram and that further investigations, preferably on oriented single crystals and by neutron scattering, are required to allow further dependable conclusions.

Conclusions

We can conclude that deviations from the equiatomic composition lead to reduction in the long-range order of the As substructure in CeAsSe, reflected in XRD powder patterns by decreasing intensities and degree of splitting of the respective superstructure reflections and diminishing orthorhombic distortion. With large deviation from the ideal composition CeAsSe, both indications of the As order within cis−trans chains disappear and are even unrecognizable by high-resolution diffraction experiments using synchrotron radiation; thus, powder diagrams can be indexed on the basis of the tetragonal subcell. We ascribe this finding to disorder introduced by breaking of covalent bonds within ideally infinite As chains by electronic deviations from $(Ce^{3+})(As^{-})(Se^{2-})$. These are introduced even by minimal deviations from the equiatomic composition within the semiconducting material. However, from the obtained data, we cannot discriminate a homogeneity range of CeAsSe within the ranges of observed compositions and the possibility of very narrow homogeneity ranges of a series of individual phases without any doubt.[23]

Acknowledgment. We thank Dr. Gudrun Auffermann, Anja Völzke, and Ulrike Schmidt for performing the CA, Dr. Ulrich Burkhardt and Thorsten Vogel for the metallographic preparations, Ralf Koban for the measurements of the electric and magnetic properties, and Monika Eckert and Petra Scheppan for the EDXS and WDXS analyses. Technical support by Irene Margiolaki at the beamline ID31 (ESRF, Grenoble) and assistance with XAS experiments by Dr. Edmund Welter and Dr. Dariusz Zajac at the beamline E4 (HASYLAB, Hamburg) is gratefully acknowledged.

Supporting Information Available: CIF files for the structure refinements. This information is available free of charge via the Internet at http://pubs.acs.org.

IC802246G

(23) Doert, T.; Graf, C.; Schmidt, P.; Vasilyeva, I. G.; Simon, P.; Carrillio-Cabrera, W. *J. Solid State Chem.* **2007**, *180*, 496–509.
(24) Parthé, E.; Gelato, L. M. *Acta Crystallogr.* **1984**, *A40*, 169–183.
(25) Gelato, L. M.; Parthé, E. *J. Appl. Crystallogr.* **1987**, *20*, 139–143.